INTERNATIONAL JOURNAL FOR NUMERICAL METHODS IN FLUIDS, VOL. 24, 1185–1210 (1997)

LOCALIZATION OF HOPF BIFURCATIONS IN FLUID FLOW PROBLEMS

A. FORTIN,[1,*] M. JARDAK,[1] J. J. GERVAIS[2]
AND R. PIERRE[2]

[1] *Département de Mathématiques et de Génie Industriel, École Polytechnique de Montréal, CP 6079, Succ. 'Centre-ville', Montréal H3C 3A7, Canada*
[2] *Département de Mathématiques et de Statistiques, Université Laval, Québec G1K 7P4, Canada*

SUMMARY

This paper is concerned with the precise localization of Hopf bifurcations in various fluid flow problems. This is when a stationary solution loses stability and often becomes periodic in time. The difficulty is to determine the critical Reynolds number where a pair of eigenvalues of the Jacobian matrix crosses the imaginary axis. This requires the computation of the eigenvalues (or at least some of them) of a large matrix resulting from the discretization of the incompressible Navier–Stokes equations. We thus present a method allowing the computation of the smallest eigenvalues, from which we can extract the one with the smallest real part. From the imaginary part of the critical eigenvalue we can deduce the fundamental frequency of the time-periodic solution. These computations are then confirmed by direct simulation of the time-dependent Navier–Stokes equations.

Int. J. Numer. Meth. Fluids, **24**: 1185–1210, 1997.

No. of Figs: 27. No. of Tables: 3. No. of Refs: 33.

KEY WORDS: Hopf bifurcation; hydrodynamic stability; Navier–Stokes equations; eigenproblem; direct simulation

1. INTRODUCTION

It has become relatively easy to compute solutions of complex fluid flow problems by means of numerical methods. Two- and three-dimensional stationary problems can now be studied on very fine meshes, although to a lesser extent in 3D. Solutions can be computed at large Reynolds numbers in various geometries. However, it is not always clear whether these solutions are stable in the linear hydrodynamic sense.

In very simple geometries such as Poiseuille or Couette flows, linear stability can be easily established by reducing the problem to one dimension using the Orr–Sommerfeld equations.[1] However, in more general geometries this is no longer a simple task.

There are at least two ways to verify the stability of a stationary solution. The first one consists of performing a direct simulation by solving the time-dependent Navier–Stokes equations, starting near the stationary solution, and of verifying whether the corresponding time-dependent solution goes back to the stationary solution after a certain transition time. Such a computation is rather expensive in computational time but was nevertheless used by Fortin *et al.*[1,2] in the case of the flow around a

* Correspondence to: A. Fortin.

CCC 0271–2091/97/111185–26 $17.50

Received 11 July 1995
Revised 11 March 1996

periodic array of cylinders and by Goodrich *et al.*[3] and Gustafson and Halasi[4,5] for the driven cavity flow at different Reynolds numbers and aspect ratios.

The second approach requires the computation of the eigenvalues (or at least some of them) of a large matrix corresponding to the linearization of the discretized Navier–Stokes equations (the Jacobian matrix) in the neighbourhood of the stationary solution. Although large-matrix eigenproblems are rather difficult, this approach was successfully applied in some problems.[6–8]

In this paper we study linear hydrodynamic stability using a combination of the two approaches and we apply the resulting method to a wide variety of two-dimensional incompressible flow problems to establish its flexibility. We also discuss briefly the inherent difficulties associated with the implementation of known methods for the computation of eigenvalues in the finite element context. Finally, numerical results are presented for the lid-driven cavity (regularized or not), backward-facing step and periodic grooved channel problems.

2. MATHEMATICAL SETTING

The two-dimensional time-dependent incompressible Navier–Stokes equations in primitive variables are written as

$$\begin{aligned} &\frac{\partial \mathbf{v}}{\partial t} - \frac{1}{Re}\nabla \cdot [2\dot{\boldsymbol{\gamma}}(\mathbf{v})] + (\mathbf{v}\cdot\nabla)\mathbf{v} + \nabla q = 0, \\ &\nabla \cdot \mathbf{v} = 0, \qquad \mathbf{v}|_{\mathbf{x}\in\Gamma} = \mathbf{g}, \qquad \mathbf{v}(\mathbf{x},0) = \mathbf{v}_0(\mathbf{x}). \end{aligned} \tag{1}$$

As usual, $\mathbf{v}$ is the velocity field, p is the pressure and $\dot{\boldsymbol{\gamma}}(\mathbf{v}) = [\nabla\mathbf{v} + (\nabla\mathbf{v})^{\mathrm{T}}]/2$ is the rate-of-strain tensor. Boundary and initial conditions depend of course on the problem and will be made precise later on. For the sake of simplicity we consider only Dirichlet boundary conditions, but as we shall see in the applications, more general boundary conditions can be considered.

To study the linear hydrodynamic stability of a steady solution $(\bar{\mathbf{U}}, \bar{p})$, we look for solutions $(\mathbf{v}, q)$ of (1) of the form

$$\mathbf{v}(\mathbf{x},t) = \bar{\mathbf{U}}(\mathbf{x}) + \mathrm{e}^{\sigma t}\mathbf{u}(\mathbf{x}), \qquad q(\mathbf{x},t) = \bar{p}(\mathbf{x}) + \mathrm{e}^{\sigma t}p(\mathbf{x}). \tag{2}$$

Substituting in (1) and neglecting second-order terms, one easily obtains the eigenvalue problem

$$\begin{aligned} -\frac{1}{Re}\nabla \cdot [2\dot{\boldsymbol{\gamma}}(\mathbf{u})] + (\bar{\mathbf{U}}\cdot\nabla)\mathbf{u} + (\mathbf{u}\cdot\nabla)\bar{\mathbf{U}} + \nabla p &= -\sigma\mathbf{u}, \\ \nabla\cdot\mathbf{u} = 0, \qquad \mathbf{u}|_{\mathbf{x}\in\Gamma} &= 0, \end{aligned} \tag{3}$$

where $\sigma = \sigma^{\mathrm{r}} + \mathrm{i}\sigma^{\mathrm{i}}$ is a complex eigenvalue. The solution of (3) gives the normal mode $\mathrm{e}^{\sigma t}(\mathbf{u}(\mathbf{x}), p(\mathbf{x}))$. The least stable mode is the normal mode corresponding to the rightmost eigenvalue. From (2) it is easily seen that instability will occur if the real part σ^{r} of one of the eigenvalues σ becomes positive. In that case the perturbation of the stationary solution will grow exponentially. When one pair of conjugate complex eigenvalues crosses the imaginary axis as Re increases, we generically encounter a Hopf bifurcation: the stationary solution loses its stability and a one-parameter family of periodic solutions bifurcates from the stationary solution. If the bifurcation is supercritical, i.e. the branch of periodic solutions bifurcates in the direction of increasing Reynolds number, the bifurcating solutions are stable. Moreover, the amplitudes of the periodic solutions are $O(|Re - Re_{\mathrm{cr}}|^{1/2})$,[9] where Re_{cr} is the critical Reynolds number for which a Hopf bifurcation occurs. This paper is concerned with the determination of Re_{cr}.

2.1. Variational formulation

We define on Ω (a bounded domain of $\mathbb{R}^2$) the space

$$H_0^1(\Omega) = \{u | u \in L^2(\Omega), \nabla u \in (L^2(\Omega))^2, u|_{\mathbf{x}\in\Gamma} = 0\},$$

$$\mathscr{X} = (H_0^1(\Omega))^2, \qquad \mathscr{Q} = L_0^2(\Omega) = \left\{ q \in L^2(\Omega) \middle| \int_\Omega q \mathrm{d}x = 0 \right\}.$$

The variational formulation of problem (3) can be written in the following mixed form:

$$\begin{gathered} \text{find } \sigma \in \mathbb{C}, (\mathbf{u}, p) \in \mathscr{X} \times \mathscr{Q}, (\mathbf{u}, p) \neq (0,0) \text{ such that} \\ a_{\bar{\mathbf{U}}}(\mathbf{u}, \mathbf{v}) - b(\mathbf{v}, p) = -\sigma(\mathbf{u}, \mathbf{v}) \quad \forall \mathbf{v} \in \mathscr{X}, \qquad b(\mathbf{u}, q) = 0 \quad \forall q \in \mathscr{Q}, \end{gathered} \tag{4}$$

where

$$a_{\bar{\mathbf{U}}}(\mathbf{u}, \mathbf{v}) = \frac{1}{Re} \int_\Omega \dot{\boldsymbol{\gamma}}(\mathbf{u}) : \dot{\boldsymbol{\gamma}}(\mathbf{v}) \, \mathrm{d}\mathbf{x} + \int_\Omega [(\mathbf{u} \cdot \nabla)\bar{\mathbf{U}} \cdot v + (\bar{\mathbf{U}} \cdot \nabla)\mathbf{u} \cdot \mathbf{v}] \, \mathrm{d}\mathbf{x},$$

$$b(\mathbf{u}, q) = \int_\Omega \nabla \cdot \mathbf{u} \, q \mathrm{d}\mathbf{x}.$$

For the sake of completeness we give the conditions for the existence and uniqueness of the triplet $(\sigma, \mathbf{u}, p)$.[10]

1. The bilinear form $a_{\bar{\mathbf{U}}}(.,.)$ must be continuous on $\mathscr{X} \times \mathscr{X}$. This can be established with the help of the Sobolev embedding theorem.
2. The bilinear form $b(.,.)$ must also be continuous on $\mathscr{X} \times \mathscr{Q}$ and verify the Brezzi–Babŭska inf-sup condition.[11]
3. Finally, the bilinear form must satisfy the Gårding inequality:

$$\begin{gathered} \text{there exist two positive constants } \gamma \text{ and } \alpha \text{ such that} \\ a_{\bar{\mathbf{U}}}(\mathbf{v}, \mathbf{v}) + \gamma |\mathbf{v}|_{0,\Omega}^2 \geqslant \alpha \|\mathbf{v}\|_{1,\Omega}^2 \quad \forall \mathbf{v} \in \mathscr{X}, \end{gathered} \tag{5}$$

   where $|.|_{0,\Omega}$ is the $L^2(\Omega)$ norm and $\|.\|_{1,\Omega}$ is the norm on $\mathscr{X}$.

It is also possible to formulate the problem in a simpler way. Introducing the space of divergence-free functions,

$$\mathscr{V} = \{\mathbf{v} \in \mathscr{X} \text{ such that } \nabla \cdot \mathbf{v} = 0\},$$

problem (4) can also be written as:

$$\begin{gathered} \text{find } \sigma \in \mathbb{C}, \mathbf{u} \in \mathscr{V}, \mathbf{u} \neq 0 \text{ such that} \\ a_{\bar{\mathbf{U}}}(\mathbf{u}, \mathbf{v}) = -\sigma(\mathbf{u}, \mathbf{v}) \quad \forall \mathbf{v} \in \mathscr{V}. \end{gathered} \tag{6}$$

The finite element discretization of such a problem results in a generalized eigenproblem of the form

$$A\mathbf{x} = -\sigma M \mathbf{x}, \tag{7}$$

where A and M are the stiffness and mass matrices respectively. In the next section we show how to compute the eigenvalues most susceptible to crossing the imaginary axis.

3. COMPUTATION OF EIGENVALUES

As the matrix in (7) is of very large size, the computation of all the eigenvalues would be prohibitive. The critical eigenvalue is the first one to cross the imaginary axis as *Re* increases. We only know that

its real part is zero and that its modulus is, most probably but not certainly, small (see Reference 12, Remark 2.4.1). It is therefore natural to look only at the eigenvalues with smallest modulii. This can be done with the help of the simultaneous inverse iteration method described by Jennings,[13] which allows the computation of the n_e smallest eigenvalues. We have to guess the number of eigenvalues to compute in order to obtain the critical one. This is the major weakness of the proposed method and will be discussed more fully at the end of this section.

We now give a brief description of the algorithm, referring the reader to References 13 and 14 for more details.

1. Construct a set of m random trial vectors
$$U_0 = (\mathbf{u}_1, \mathbf{u}_2, \ldots, \mathbf{u}_m),$$
which is orthonormalized by a modified Gram–Schmidt procedure.
2. For $k \geqslant 1$ solve the m linear systems
$$AV_k = MU_k.$$
3. Construct the iteraction matrix
$$B_k = U_k^{\mathrm{T}} V_k.$$
4. Compute the eigenvalues of B_k by the QR method:
$$B_k P_k = P_k \Lambda_k,$$
where Λ_k is the diagonal matrix containing the eigenvalues.
5. Invert and sort (by increasing modulus) the eigenvalues of B_k.
6. Compute the eigenvectors
$$W_k = V_k P_k.$$
7. Orthonormalize W_k by the modified Gram–Schmidt method. These new orthonormal vectors become the columns of the new (updated) matrix U_k.
8. Perform a convergence test on the eigenvalues. If it fails, return to step 2.

The number m of starting trial vectors is set to $n_e + 8$ according to Bathe and Wilson.[15] This particular choice enhances the convergence of the algorithm. It is worth noticing that the m column vectors of V_k in step 2 should be divergence-free. More precisely, these vectors should be divergence-free in a discrete (finite element) sense denoted as $\nabla_h \cdot \mathbf{v} = 0$.[11] To achieve this, a Uzawa algorithm[16] is used to solve the m linear systems occurring in step 2. For each column vector $\mathbf{v}_l$, $l = 1, 2, \ldots, m$, this gives the following algorithm.

0) Initialization: $(\mathbf{v}_{l,0}, p_{l,0})$ given arbitrarily.
1) Iterations: for $n \geqslant 0$, $(\mathbf{v}_{l,n}, p_{l,n})$ being known, find $\delta\mathbf{v}_n$ satisfying

$$\int_\Omega \left(\frac{2}{Re} \dot{\boldsymbol{\gamma}}(\delta\mathbf{v}_n) : \dot{\boldsymbol{\gamma}}(\mathbf{w}) + (\bar{\mathbf{U}} \cdot \nabla)\delta\mathbf{v}_n \cdot \mathbf{w} + (\delta\mathbf{v}_n \cdot \nabla)\bar{\mathbf{U}} \cdot \mathbf{w} + r_1(\nabla_h \cdot \delta\mathbf{v}_n)(\nabla_h \cdot \mathbf{w}) \right) \mathrm{d}x$$
$$= \int_\Omega \left(\frac{2}{Re} \dot{\boldsymbol{\gamma}}(\mathbf{v}_{l,n}) : \dot{\boldsymbol{\gamma}}(\mathbf{w}) + (\bar{\mathbf{U}} \cdot \nabla)\mathbf{v}_{l,n} \cdot \mathbf{w} \right) \mathrm{d}x$$
$$+ \int_\Omega [(\mathbf{v}_{l,n} \cdot \nabla)\bar{\mathbf{U}} \cdot w + p_{l,n}(\nabla_h \cdot \mathbf{w}) + r_1(\nabla_h \cdot \mathbf{v}_{l,n})(\nabla_h \cdot \mathbf{w}) - \mathbf{u}_l \cdot \mathbf{w}] \, \mathrm{d}x.$$

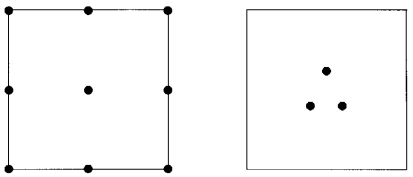

Figure 1. Q_2–P_1 element

2) Update:

$$\mathbf{v}_{l,n+1} = \mathbf{v}_{l,n} - \delta\mathbf{v}_n, \qquad p_{l,n+1} = p_{l,n} - r_1 \nabla_h \cdot \mathbf{v}_{l,n+1}.$$

3) Convergence test.

The constraint

$$\nabla_h \cdot \mathbf{v}_l = 0$$

in each problem of step 2 is imposed through the Lagrange multiplier p_l (the pressure). The penalization parameter r_1 is set to 10^7. The Q_2–P_1 element of Figure 1 was chosen for the discretization of the velocities and pressure respectively. This element is one of the best for two-dimensional computations. In fact, this element is second-order in space ($O(h^2)$) and satisfies the discrete inf-sup condition as described in Reference 17.

The choice of an appropriate mixed finite element discretization for the detection of bifurcations of incompressible fluids has not received a lot of attention. In a recent paper, Gervais *et al.*[7] have conducted a series of experiments on the influence of the discretization on the prediction of the dynamical behaviour of the lid-driven cavity flow. In this work they have used a stationary code coupled with subspace iteration to monitor the evolution of the spectrum as the Reynolds number increases. The main conclusions of their work are that linear finite elements are too diffusive and local mass conservation (i.e. at the element level) seems to play an important role in the precision of the predicted critical values. In this respect, C^{-1} pressure approximations have all the necessary qualities and, among all possible choices, the Q_2–P_1 element is considered to be one of the best.

In the course of the above-mentioned research effort the last two authors have also tested various modifications of the subspace iteration algorithm in the hope of reducing the workload associated with the fact that a direct use of the above algorithm requires the determination of the p smallest eigenvalues, where p can be rather large. Even if the discretizations used there were different from the one employed here, we believe that in the lid-driven cavity case the conclusions remain the same. It might be worth noticing, however, that the computation of a larger part of the spectrum may reveal interesting features of the flow which would otherwise be missed.

The first modification that was studied, which has been advocated by several authors,[18,19] involves Mobius conformal transformation of the complex plane and leads one to work with an appropriate Cayley transform of A in lieu of A itself. All the variants that we have tested failed. The reason for this failure may be related to the mapping properties of the Mobius transform itself. Roughly speaking, what one aims at when using this transform is to map a vertical half-plane $Re(z) > a$, containing the spectrum of A, onto the unit disc with the point at infinity going onto the point one. The value of a is chosen in such a way that the real part of the critical eigenvalue is the nearest to it, so that its image becomes the dominant eigenvalue of the corresponding Cayley transform. However, any neighbourhood of the point at infinity will then be mapped onto a lunar-like neighbourhood of one. If the spectrum of A comprises eigenvalues of large modulus, its Cayley transform will have a spectrum with a dominant eigenvalue near the unit circle and a large cluster of unwanted eigenvalues

very near the point one, the worst case being the one for which some of the large eigenvalues have a real part near that of the critical eigenvalue. The rate of convergence of these eigenvalues will be so near one that it will be almost impossible to kill the corresponding components of the eigenvectors in any reasonable time. As we shall show, the lid-driven cavity corresponds to such a spectrum structure and even the clever method proposed by Cliffe *et al.*[18] did not seem applicable. However, as demonstrated by Gresho *et al.*,[6] this approach proved very useful for the backward-facing step case.

The second very interesting alternative that has been considered is the modification of the iterative procedure resulting from the replacement of the powers of A by some other polynomial transformation. The choice of the transform, often called a filter, is dictated by the part of the spectrum that one wants to separate from the critical eigenvalue. In References 20 and 21 the use of Chebychev polynomials is advocated for the problem of determining the leftmost or rightmost eigenvalues. This possibility was tested with the help of the EB12 code of Duff and Scott,[22] in which this type of filter is combined with subspace iteration. The method seems to work fine for the lid-driven cavity problem as long as the desired eigenvalues are simultaneously the rightmost (leftmost) and those of largest modulus. Unfortunately, this is not the case in our situation and after a period of wild oscillations, the code generates worthless approximations with warnings of insufficient precision, regardless of the number of guard vectors that we use. This does not seem to be related to the code itself, which works very well in various situations involving small matrices.

There could be problems of an algorithmic nature associated with the fact that we try to work in the divergence-free velocity subspace. To challenge this idea, we have implemented the modification of the eigenvalue problem suggested by Cliffe *et al.*,[23] which requires us to work in the whole space and to control the spurious eigenvalues associated with the use of the Lagrange multiplier. Our attempt to generate the leftmost eigenvalues of that problem with the help of EB12 met with success when we used small meshes but failed on finer ones. Again, this seems to be related to the structure of the spectrum itself: for the lid-driven cavity problem there are a lot of unwanted eigenvalues in a narrow vertical band containing the critical one, some of them with larger imaginary part. It could be that in such a situation the determination of the ellipses used to define the Chebychev polynomials is an ill-conditioned problem. Although this possibility is evoked by Saad[20] himself, we do not have any theoretical arguments to support it. As far as we are concerned, the correct implementation of those ideas in the lid-driven cavity case is still an open question on which we are currently working.

There is one last point which deserves some comment. It concerns the possibility of improving the approximation of the critical value of the Reynolds number by considering an extended system. One such approach is proposed by Griewank and Reddien.[24] The reason why we could not consider such an approach is purely algorithmic: in the process of determining the spectrum of the matrix A, the only thing that we can safely do is multiply A^{-1} by a vector. We do not even have A at hand, since its explicit construction would require the knowledge of a basis of the subspaces of discrete velocity field satisfying

$$\nabla_h \cdot \mathbf{v}_h = 0.$$

We do not know of any such basis. This fact alone forbids the use of any method requiring the construction of A^2 or the factorization of A or its reduction to Hessenberg form as suggested by Grienwank and Reddien.[24] These methods are quite useful for problems involving medium-sized matrices. Their implementation in the finite element context will, however, require further investigations into matrix-free methods of resolution of the extended system.

In view of the above-quoted difficulties, our approach does not allow us to be very affirmative about the critical nature of the bifurcation, since we might very well have missed a preceding one. To get around that problem, it was simpler for us to use direct simulation as described in the next section.

4. DIRECT SIMULATIONS

To ascertain the results of our eigenvalue computations, direct simulations will also be presented consisting of solving the time-dependent Navier–Stokes equation (1), starting with some initial condition (usually from rest).

The numerical methodology for direct computation is similar to the one used for the computation of the eigenvalues. A method based on a combination of the Uzawa algorithm and Newton–Raphson as introduced in Reference 25 is used to solve the non-linear incompressible Navier–Stokes equations. The time discretization is performed using a fully implicit second-order Gear scheme. The reader is referred to References 1 and 2 for a complete description of the numerical methodology.

During the simulation the velocity signal $v(t)$ at some points in the domain is stored. Approximately 100,000 time steps are performed and the first time steps are eliminated since they correspond to the transient state. The last 2^{16} points are then used for the construction of the phase portraits and for the Fourier analysis.

The phase portrait is simply a plot of $v(t)$ versus $v(t+T)$, where T is an almost arbitrary time delay. If the signal $v(t)$ is periodic, T should be chosen in an appropriate way, in particular far enough from the period of the signal, to avoid a phase portrait compressed along the diagonal. With a proper choice for T a periodic signal will result in a closed curve in the phase portrait. Finally, the Fourier analysis allows the computation of the fundamental frequency f_1 of the signal $v(t)$, which, in view of the Hopf bifurcation theorem,[9] can be deduced from the imaginary part of the critical eigenvalue through the relation

$$\sigma^i_{\mathrm{cr}} = 2\pi f_1 + O(Re - Re_{\mathrm{cr}}).$$

This last equation makes it possible to compare the eigenvalue computation with the direct simulation.

5. NUMERICAL RESULTS

We now present numerical results for various problems. In each case we will specify the number of computed eigenvalues necessary to obtain the critical one. We will also specify the critical Reynolds number, plot the least stable mode and verify our results by direct computation using our time-dependent Navier–Stokes solver.

In all applications the strategy is the following.

1. For a given Reynolds number a stationary solution is computed.
2. This stationary solution is then injected into the eigenproblem (7) and a number of eigenvalues are then computed.
3. If no eigenvalue is on the right of the real axis, the Reynolds number is increased and we return to step 1.
4. If one pair of eigenvalues has a positive real part, the Reynolds number is reduced (using a bisection method) until we find the critical Reynolds number Re_{cr}.
5. When the critical Reynolds number has been located, a direct simulation is performed by solving the time-dependent Navier–Stokes equations at Reynolds numbers around Re_{cr}.
6. Comparisons are made between the frequency of the periodic solution and the imaginary part of the critical eigenvalue.

5.1. Poiseuille flow

The above strategy has first been tested on the Poiseuille flow. The critical Reynolds number was found to be 5772, in very good agreement with classical results.[26] The complete results are reported in Reference 1.

5.2. Square lid-driven cavity

The square cavity problem is probably one of the most standard test problems used for the analysis of numerical methods for the Navier–Stokes equations. Although it is not possible to give an analytical solution, the geometry is so simple that most numerical codes have been tested on this problem, since it is easy to make comparisons with existing results in the literature. Solutions at relatively large Reynolds numbers can now be computed with high precision. The question of the stability of these solutions has been raised a few times[7,27] and we will try to give a complete analysis.

In this problem, Ω is the unit square $]0, 1[\times]0, 1[$ of Figure 2. We assume the boundary conditions

$$\mathbf{u}(x, y) = \begin{cases} (0, 0) & \text{if } y < 1, \\ (1, 0) & \text{if } y = 1, \end{cases}$$

The boundary conditions are singular at the upper corners. We have assumed that the velocity is (1, 0) on the top wall, including both corners.

Previous studies have shown the presence of a Hopf bifurcation, but its precise location (Re_{cr}) is still unknown. Bruneau and Jouron[28] observed transition to turbulence for a Reynolds number lower than 7500 by solving the Navier–Stokes equations with a high-resolution grid. However, their methodology seems questionable, since they draw their conclusions by looking at how their stationary numerical solution diverges at high Reynolds numbers. Gustafson and Halasi[4] found persistent oscillations (periodic solution) for $Re < 10{,}000$ by solving the time-dependent Navier–Stokes equations. They mention that the critical Reynolds number is somewhere between 5000 and 10,000. We will try to determine this critical number more precisely by solving the eigenvalue problem (3).

Since the choice of mesh is an important issue, we have used four different meshes as illustrated in Figure 3. The numbers of elements and degrees of freedom (DOF) are summarized in Table I.

Each grid was refined near the walls to capture the main features of the flow. For example, a steady solution at $Re = 8000$ was computed with mesh 4 and is presented in Figure 4. Zooming of the top left, bottom left and bottom right of the cavity shows the presence of important corner vortices.

For each mesh we have computed the 250 smallest eigenvalues in modulus. The number 250 was obtained by trial and error until we found a pair of eigenvalues close to the imaginary axis. For

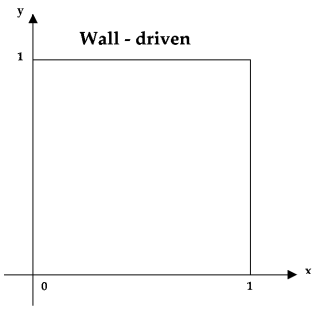

Figure 2. Geometry of lid-driven cavity

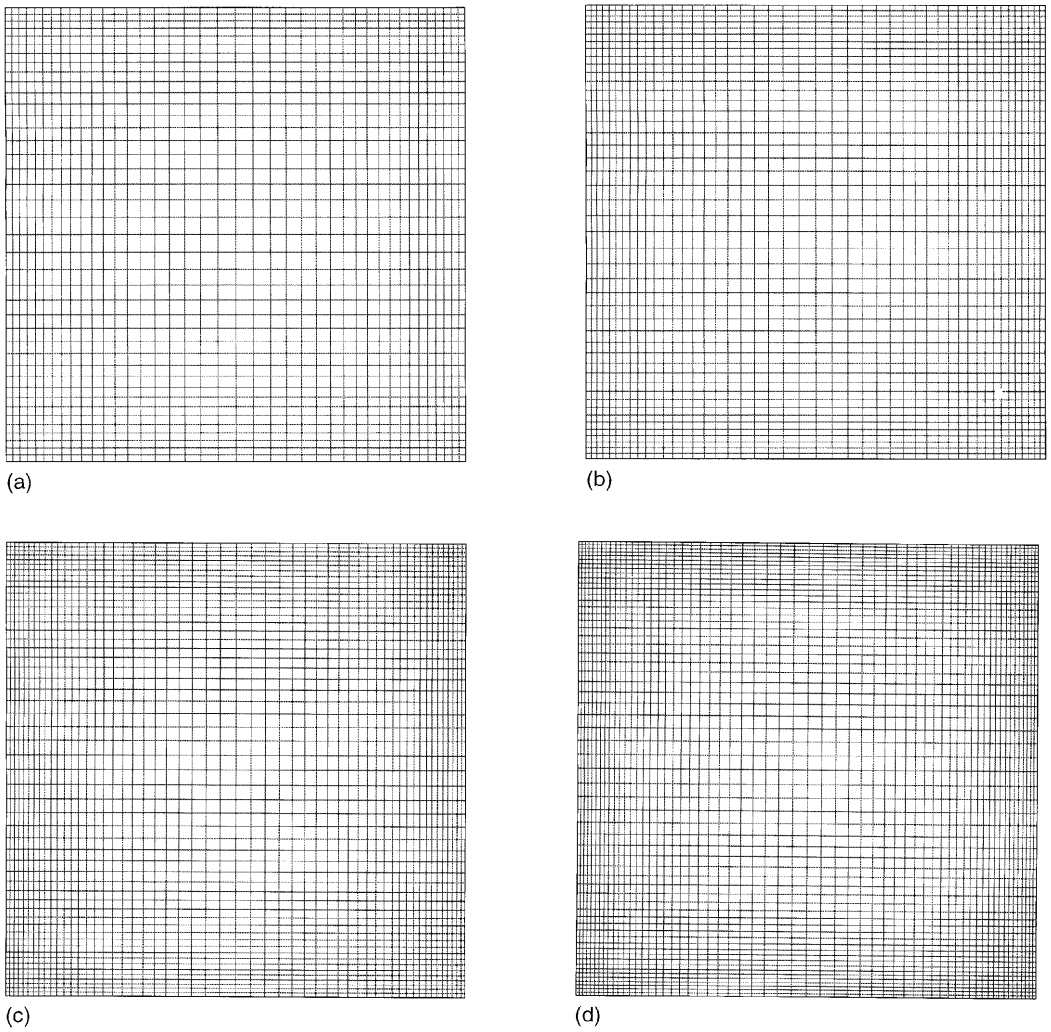

Figure 3. Meshes (a) 1, (b) 2, (c) 3 and (d) 4 for lid-driven cavity

example, the computed spectrum for $Re = 8000$ and mesh 4 is presented in Figure 5, where the critical pair of eigenvalues can be clearly seen. Many other pairs of eigenvalues are very close to the imaginary axis, but only one pair crosses the axis if the Reynolds number is slightly increased. The real and imaginary parts of the eigenvector corresponding to the critical eigenvalue and also illustrated in the same figure. As can be seen, the instability is more likely to start at the left wall.

Table I. Mesh parameters

	No. of elements	No. of DOF
Mesh 1	1600	14082
Mesh 2	2116	18678
Mesh 3	2916	25814
Mesh 4	3600	31922

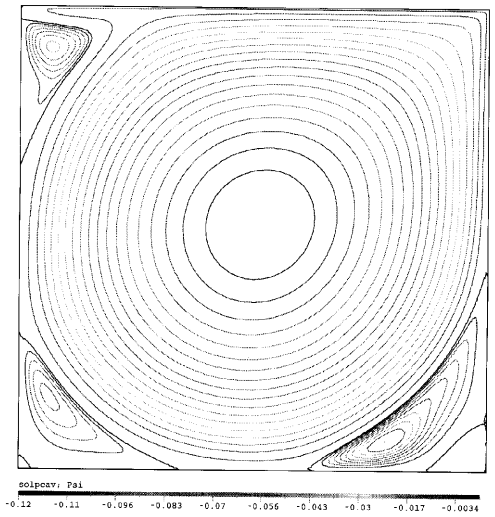

Figure 4. Square lid-driven cavity: streamlines at $Re = 8000$ (mesh 4)

The complete results are reported in Table II.

From these computations we can draw the following conclusions.

1. The critical Reynolds number Re_{cr} for the square lid-driven cavity is around 8000 (this nice number is very puzzling!).
2. We have convergence of the critical Reynolds number and critical eigenvalue with mesh refinement.
3. The imaginary part of the critical eigenvalue (which is directly related to the frequency of the periodic solution) is not very sensitive to mesh refinement.

To complete the discussion, we have also investigated the dynamical behaviour of the square lid-driven cavity by performing a direct numerical simulation of the time-dependent incompressible flow.

Starting from rest, a solution was computed at $Re = 7000$. The time step Δt was set to 0·01 and mesh 3 was used. As expected, the solution reaches a steady state after a short transition time. This is illustrated in Figure 6, where the horizontal velocity at the point (0·0147, 0·54187) (a point close to the left wall) is plotted at each time step. In contrast, $Re = 8000$, just after the Hopf bifurcation has taken place ($Re_{cr} = 7998{\cdot}5$), the numerical solution develops a time-periodic pattern as can be seen in Figure 7. This periodic solution is confirmed by the closed curve of the phase portrait of Figure 8 and by the Fourier analysis of Figure 9 (see Reference 2 for more details). From this last figure the fundamental frequency is seen to be $f_1 = 0{\cdot}45166$. The relation between f_1 and the imaginary part of the critical eigenvalue is

$$\sigma_{cr}^{i} \approx 2\pi f_1 = 2{\cdot}83786.$$

The agreement with our eigenvalue computation is very good. It can also be seen in Figure 9 that the amplitude of the fundamental frequency f_1 is very small (9×10^{-5}), supporting the conclusion that the Hopf bifurcation has just taken place and that the bifurcation is supercritical.

Let us say a few words about the periodic solution itself. A close look at the solution shows a slight pulsation of the corner vortices on the left wall. These two vortices interact among themselves, while the core of the flow remains almost stationary. The time-dependent solution is not illustrated, because

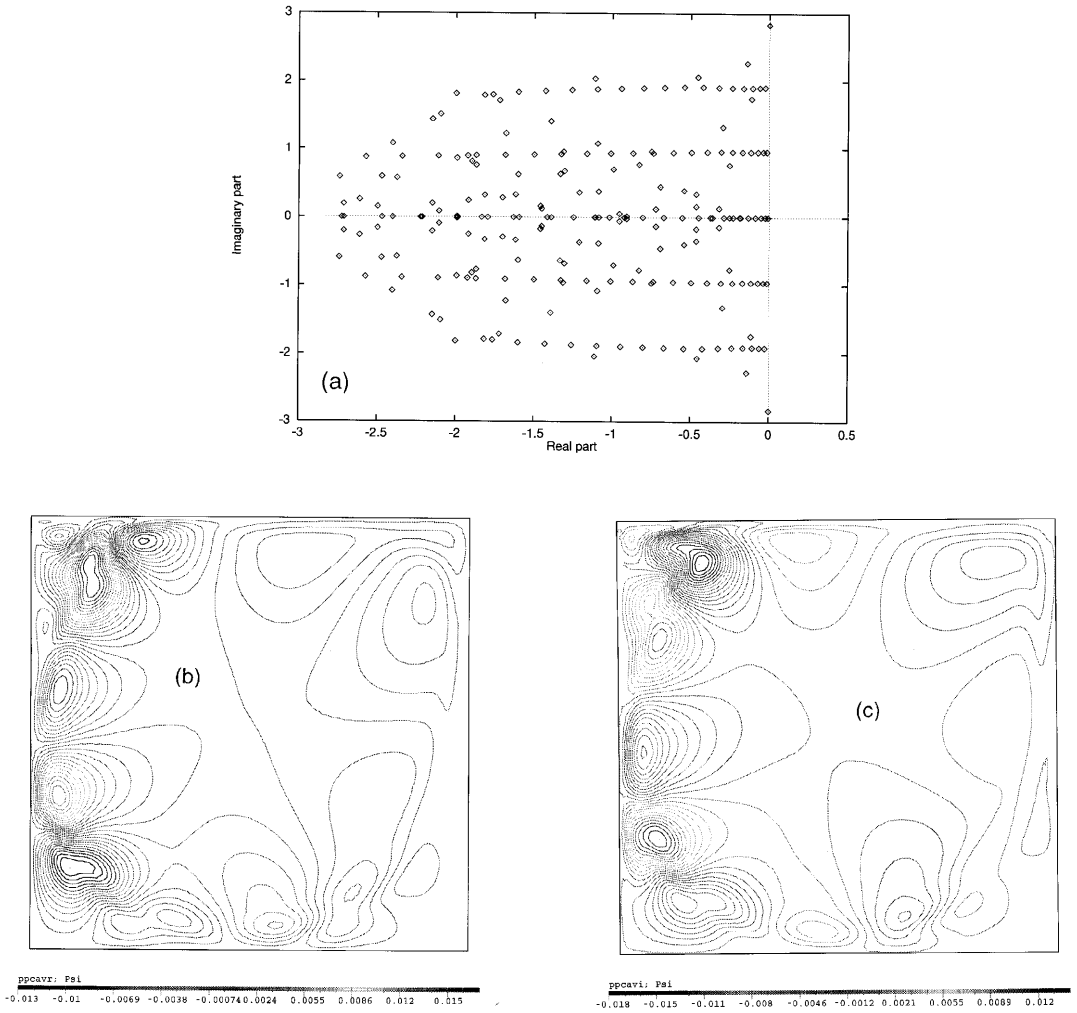

Figure 5. (a) Eigenvalues and (b) real and (c) imaginary parts of critical eigenvector

the weak amplitude of the oscillations makes the solution hardly distinguishable from the stationary solution. Of course, when the Reynolds number is further increased, the amplitude of the oscillations increases. This topic is, however, beyond the scope of this paper and we refer to Reference 10 for a complete description of the solution behaviour at higher Reynolds numbers.

5.3. Regularized square lid-driven cavity

The domain Ω is the same as in the previous problem, but the boundary conditions are now

$$\mathbf{u}(x, y) = \begin{cases} (0, 0) & \text{if } y < 1, \\ (16x^2(1-x)^2, 0) & \text{if } y = 1. \end{cases}$$

These boundary conditions reduce the effect of the singularity at the top corners, since the velocity is now continuous.

Table II. Critical eigenvalues

	Re_{cr}	Critical eigenvalue
Mesh 1	7745	$0{\cdot}38365 \times 10^{-4} \pm 2{\cdot}8741$i
Mesh 2	7937	$0{\cdot}84214 \times 10^{-4} \pm 2{\cdot}8505$i
Mesh 3	7998·5	$0{\cdot}12811 \times 10^{-4} \pm 2{\cdot}8356$i
Mesh 4	8000	$0{\cdot}54773 \times 10^{-4} \pm 2{\cdot}8356$i

A direct simulation of this flow was performed by Shen[29] using a Chebychev τ-approximation of the space variables. He concluded that the critical Reynolds number Re_{cr} was somewhere in the interval]10,000, 10,500[and that the fundamental frequency satisfies $0 \cdot 5171 \leqslant f_1 \leqslant 0 \cdot 5183$. We will try to verify these results using mesh 4 only to avoid unnecessary (and lengthy) computations.

Our eigenvalue computation led us to a critical Reynolds number $Re_{cr} \approx 10{,}255$, which agrees with the results obtained by Shen.[29] However, we found a critical eigenvalue $\sigma =$

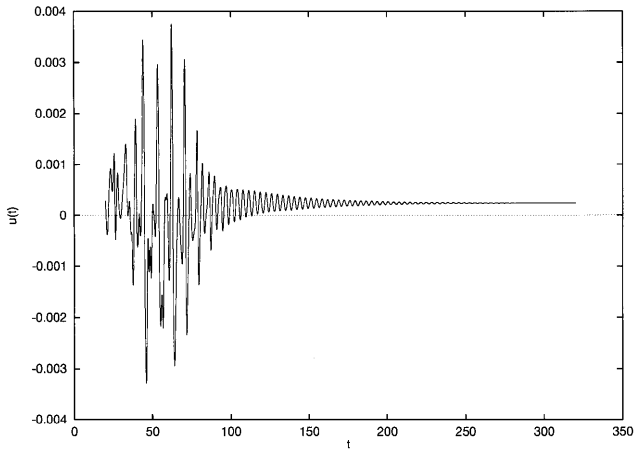

Figure 6. Time evolution at $Re = 7000$ (mesh 3)

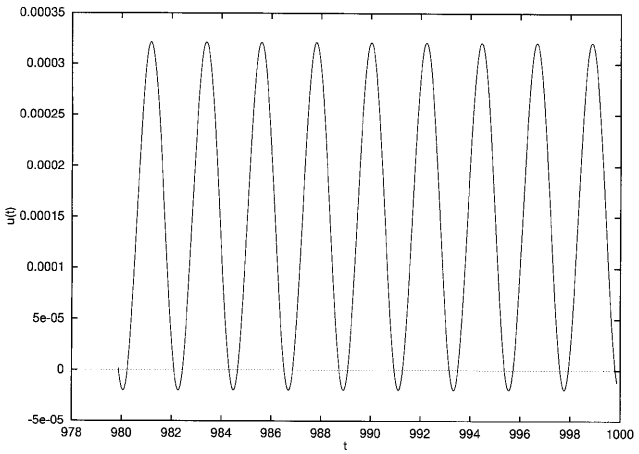

Figure 7. Time evolution at $Re = 8000$ (mesh 3)

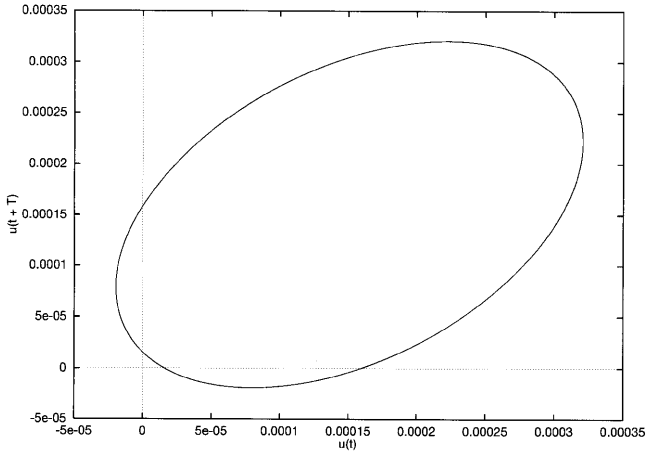

Figure 8. Phase portrait at $Re = 8000$, $T = 40\Delta t$

$0 \cdot 3309 \times 10^{-4} \pm 2 \cdot 0802\text{i}$, yielding a fundamental frequency $f_1 \approx 0 \cdot 3310637$ quite different from the value claimed by Shen. Figure 11 represents the 250 computed eigenvalues at $Re = 10{,}255$. Here again the critical pair of eigenvalues is clearly seen.

To ascertain the value of f_1, we have performed a direct simulation and made a Fourier analysis of one of the velocity components to obtain $f_1 = 0 \cdot 33112$, in excellent agreement with the critical eigenvalue. We cannot explain the difference with the results of Shen.

We give in Figure 10 the streamlines of the steady solution at $Re = 10{,}255$. As expected, the solution is similar to the one obtained at $Re = 8000$ for the previous problem, except that the present solution is smoother at both top corners. This greater regularity partly explains the difference between the critical numbers in these two problems. Another reason is that, when regularizing the boundary condition, the average velocity at the top wall reduces to one-half instead of one. After the Hopf bifurcation the behaviour of the time-dependent solution is similar to that of the regular lid-driven cavity.

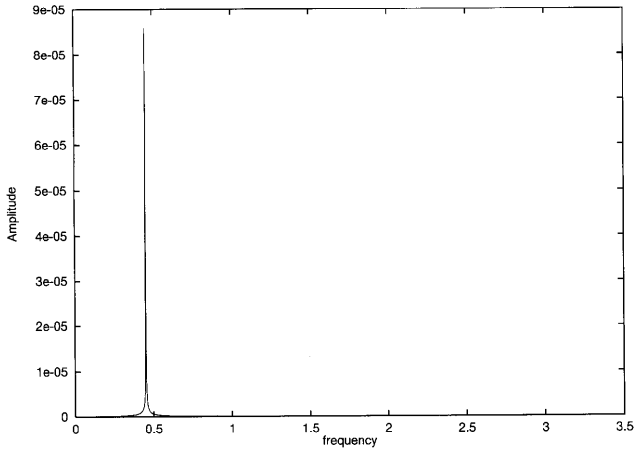

Figure 9. Fourier analysis at $Re = 8000$

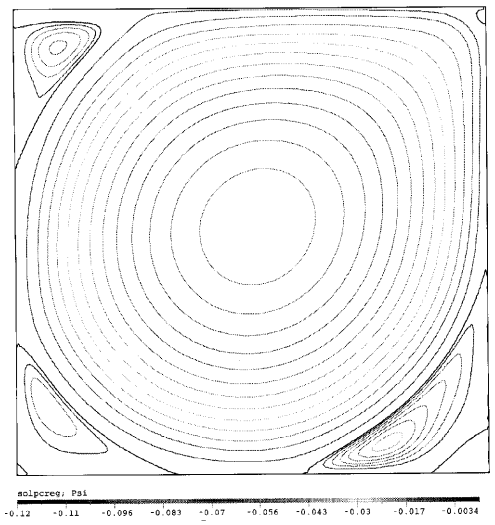

Figure 10. Regularized cavity: streamlines at $Re = 10{,}255$ (mesh 4)

A periodic solution is obtained at $Re = 10{,}258$ as illustrated in Figure 12, where we can see the signal, the Fourier analysis and the phase portrait. Here again the amplitude is very small, confirming that the Hopf bifurcation has just occurred.

5.4. Backward-facing step

We now study the flow of an incompressible fluid over the two-dimensional backward-facing step of Figure 13. This test problem has been addressed by many authors using a wide variety of numerical methods. The results are summarized in Reference 6. This last paper was an answer to a controversy concerning the stability of the stationary solution at $Re = 800$. It was claimed by Kaiktsis *et al.*[30] that it was unstable (time-periodic).In view of the following demonstration, we believe that the solution is stable at this Reynolds number and remains stable up to $Re = 1600$, where we have stopped our computations.

The domain is described in Figure 13 with $H = 1$. The fluid is allowed to enter the domain at the top half of the left side with a velocity

$$\mathbf{u}(y) = (24y(0{\cdot}5 - y), 0) \quad \text{for } 0 \leqslant y \leqslant \tfrac{1}{2},$$

mimicking the flow over a step. The Reynolds number is defined as $Re = \bar{u}H/\nu$, where $\bar{u}$ is the average inlet velocity. The usual no-slip condition is imposed on both horizontal walls, while a free (natural) boundary condition

$$[-p\mathbf{I} + 2\dot{\boldsymbol{\gamma}}(\mathbf{u})] \cdot \mathbf{n} = 0 \tag{8}$$

is (weakly) enforced on the outlet section (on the right). In Reference 6 the proposed length of the domain is $L = 15H$. As we shall see, as the Reynolds number increases, this rather short length is not consistent with the outflow boundary condition, which supposes that the flow is fully established. To confirm this hypothesis, we have also performed some computations on a longer domain ($L = 30H$).

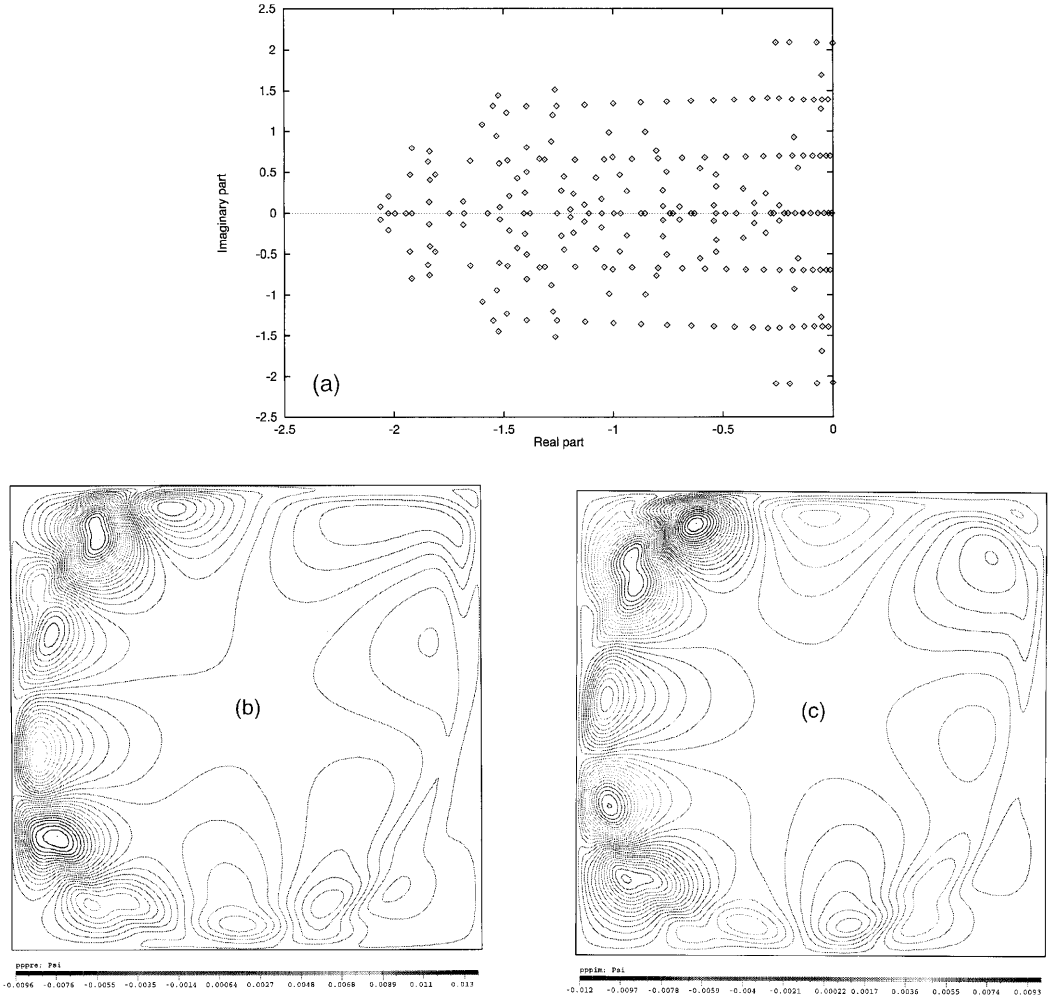

Figure 11. (a) Eigenvalues and (b) real and (c) imaginary parts of critical eigenvector

A stationary solution at different Reynolds numbers was computed using two different uniform meshes of respectively 2000 (10×200) and 4200 (14×300) elements. The horizontal and vertical components of the velocity along the axis $y = 0$ are plotted in Figure 15, showing that the flow is not fully established even at $Re = 500$ for a domain length of $15H$. Indeed, the horizontal component has not yet reached a plateau, although the vertical components seems to be zero. No important differences can be seen between the solutions on the two meshes, showing that convergence with mesh size is most probably achieved.

The situation gets worse as the Reynolds number increases, but let us recall that one of the objectives of Reference 6 was to determine an appropriate outflow boundary condition for this problem. Nevertheless, it is interesting to verify that when $L = 30H$, the same phenomenon can now be seen, but only at $Re = 1500$, as presented in Figure 16. These last solutions were computed on a uniform mesh of 4000 (10×40) elements.

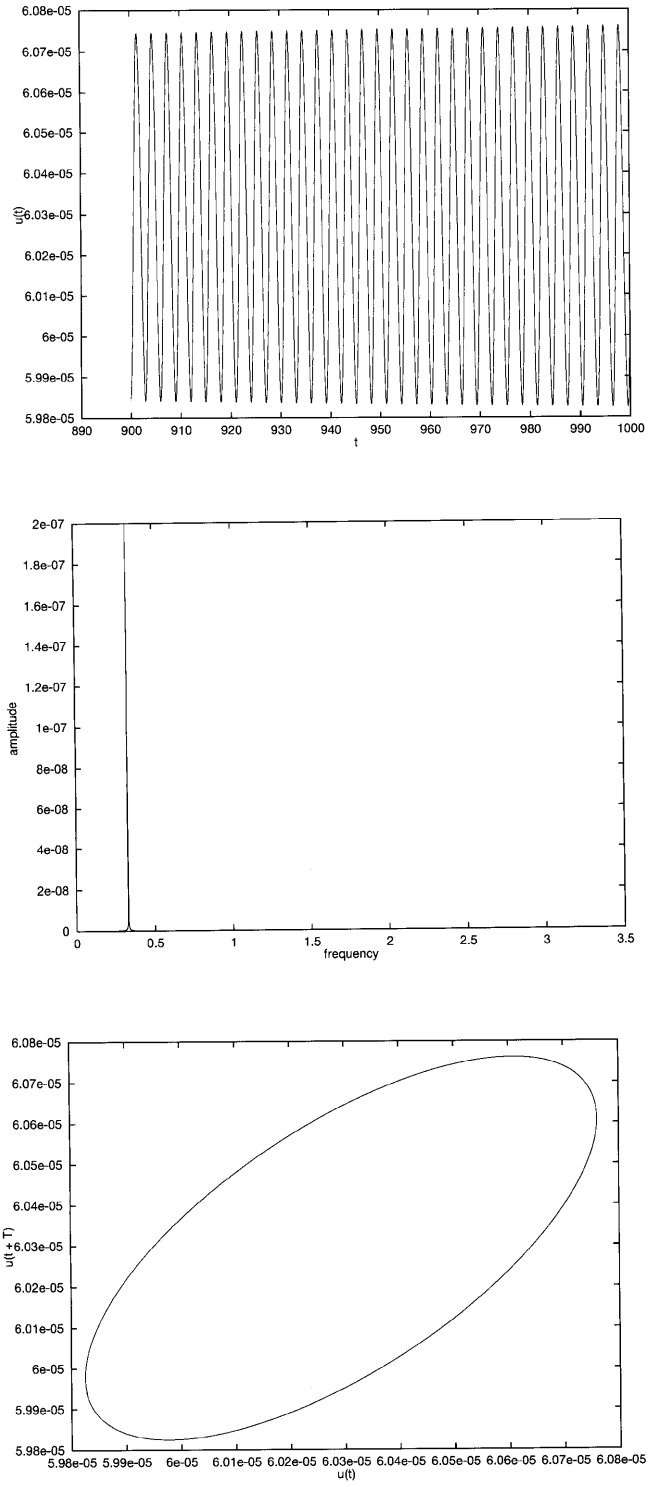

Figure 12. Regularized cavity: $Re = 10{,}258$

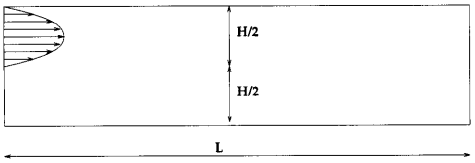

Figure 13. Geometry of backward-facing step (BFS)

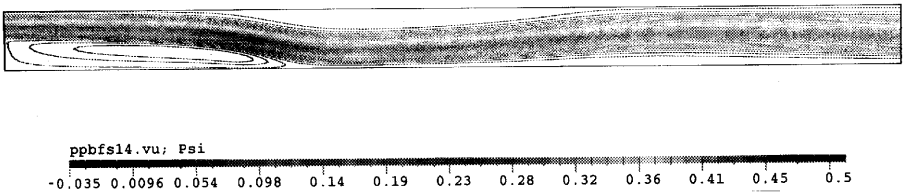

Figure 14. Stationary solution at $Re = 800$

Our stationary computations give solutions similar to those in Reference 6. For example, the solution at $Re = 800$ given in Figure 14 presents two major recirculation zones and shows, although not clearly, that the flow is not yet fully developed at the outlet.

Our direct time-dependent simulation, starting once again from rest with a time step of 0·01, tends towards the stationary solution as illustrated in Figure 17, where the streamlines are presented at different times until the flow reaches a stationary state. As shown in Figure 18, the time evolution of the horizontal velocity component taken at two different points in the domain proves that the time-dependent solution returns to its stationary state after a short transition period. Moreover, starting from the converged solution at $Re = 800$, another time-dependent simulation at $Re = 1000$ was carried out. The solution is again deemed stable.

The computation of the eigenvalues (50 in this case) presented in Figure 19 shows no eigenvalue on the imaginary axis (or even close to it). At this point we conclude, as in Reference 6, that the steady viscous incompressible two-dimensional flow over a backward-facing step at $Re = 800$ with the given outflow boundary condition is stable.

We have pushed the eigenvalue computations up to $Re = 1600$ as shown in Figure 20 and no pair of eigenvalues has crossed the imaginary axis. However, the problem is not very relevant, since we believe that the exit boundary condition is totally inadequate in this range of Reynolds numbers.

5.5. Periodic grooved channel problem

The periodic grooved channel problem was suggested by Ghaddar *et al.*[31] as a perturbation of the Poiseuille flow. This was also the case of the periodic array of cylinders studied by Fortin *et al.*[2] In the grooved channel flow the domain is supposed to be of infinite length and a groove with prescribed depth is added to perturb the flow. The details of the geometry and the dimensions are reported in Figure 21. This problem stems from the study of the cooling of computer boards and from that of compact heat exchangers.

Referring to Figure 21, a no-slip condition is imposed on the boundaries Γ_1, Γ_2 and Γ_5, while periodicity is required on the two artificial boundaries Γ_3 and Γ_4, i.e.

$$\mathbf{u}|_{\Gamma_3} = \mathbf{u}|_{\Gamma_4}.$$

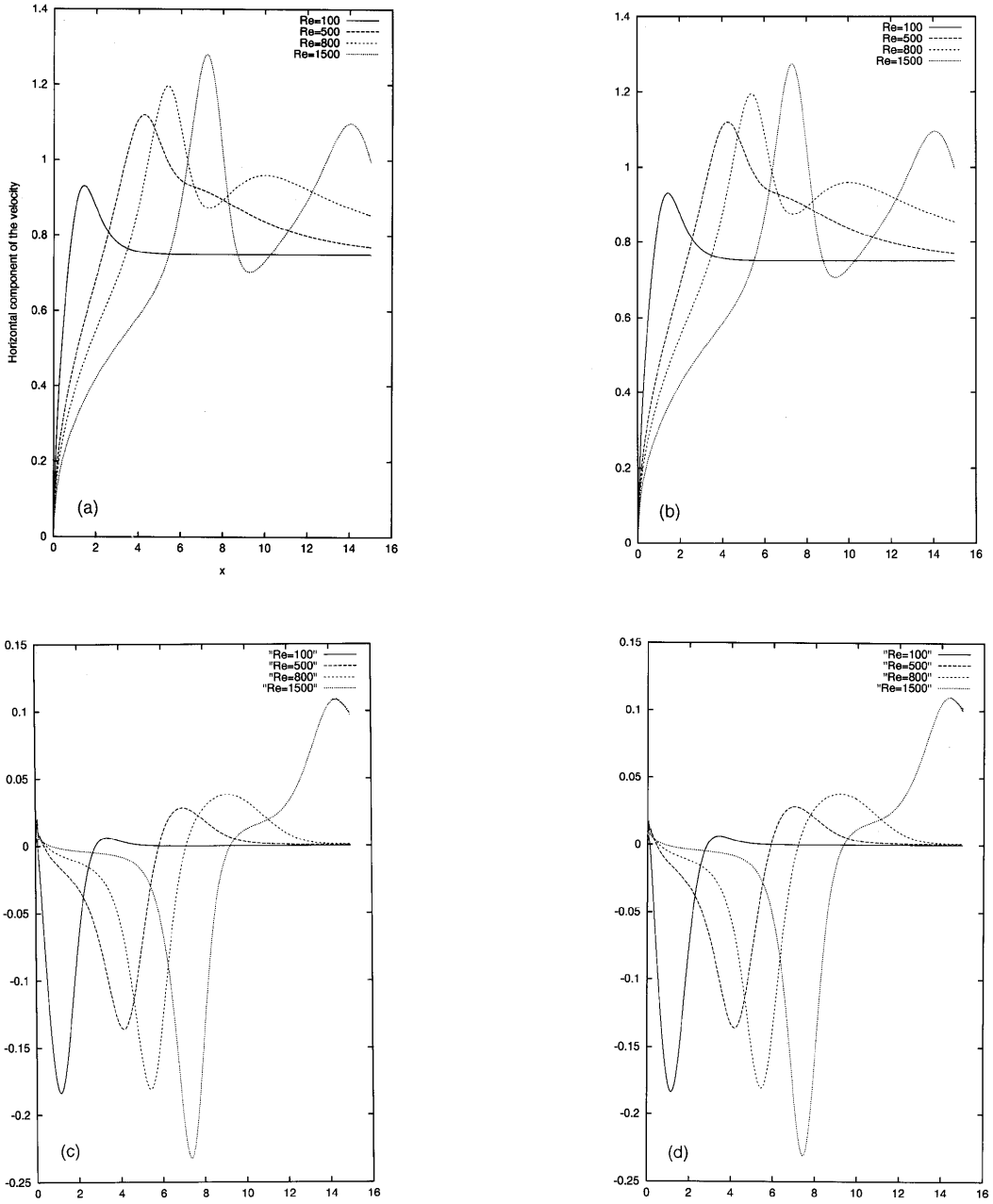

Figure 15. Velocity components ($L = 15H$) along axis $y = 0$: (a) horizontal (2000 elements); (b) horizontal (4200) elements); (c) vertical (2000 elements); (d) vertical (4200 elements)

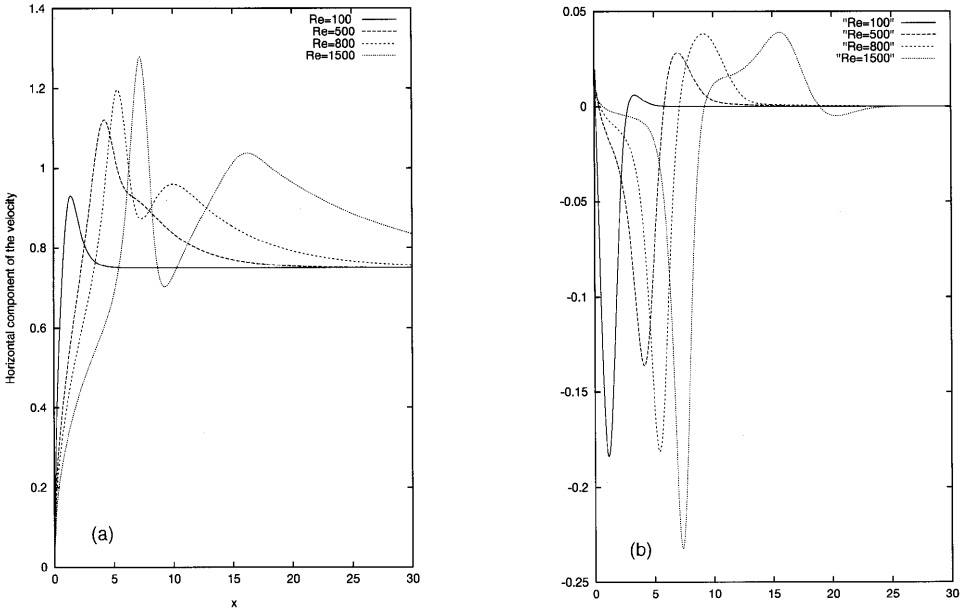

Figure 16. (a) Horizontal and (b) vertical velocity components ($L = 30H$) along axis $y = 0$

The periodicity condition also means that the velocity profile is not known *a priori* at the entrance Γ_3 of the domain. Only the total flow rate Q defined by

$$Q = \int_{\Gamma_3} \mathbf{u} \cdot \mathbf{n} \, ds$$

is known. The Reynolds number Re can then be defined as

$$Re = \frac{3hV}{2v} \quad \text{if } V = \frac{Q}{2h},$$

where v is the kinematic viscosity.

Ghaddar *et al.*[31] studied the linear stability of this flow. Their numerical investigations were based on a direct simulation of the Navier–Stokes equations linearized about a numerically calculated steady state. For each Reynolds number considered, they performed a computation of the linearized time-dependent Navier–Stokes equations. They stored the velocity signal at some points in the domain. From a plot of that signal they deduced the decay rate σ and the frequency Ω of the least stable mode. They could then obtain an approximation of the critical Reynolds number Re_{cr}. They found for the periodic grooved channel a critical Reynolds number around 900 and an approximate frequency in the neighbourhood of 0·142. Let us see what we obtain for the same problem.

A typical stationary solution is presented in Figure 22. For the computation of the eigenvalues for the grooved channel flow we used a slightly different algorithm to solve the m linear systems $AV_k = MU_k$. The periodicity condition $\mathbf{u}|_{\Gamma_3} = \mathbf{u}|_{\Gamma_4}$ should be taken care of, but the most difficult part is the imposition of the flow rate Q. We refer to Reference 32 for a complete description of how this can be done with the help of a Lagrange multiplier. We have used three different meshes as illustrated

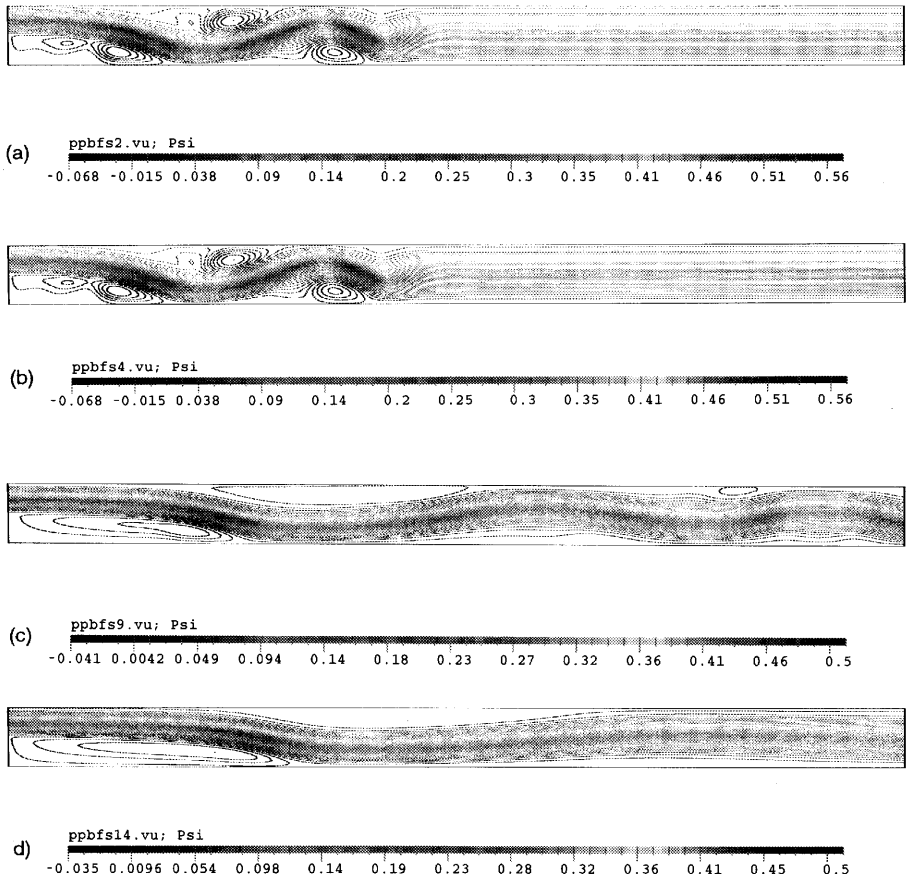

Figure 17. Streamlines at $Re = 800$: (a) $t = 10$; (*b*) $t = 20$; (c) $t = 45$; (d) $t = 140$

in Figure 23 and here again we have convergence of the critical Reynolds number and critical eigenvalue with mesh refinement. The results are summarized in Table III.

The flow loses stability at $Re_{cr} \approx 1113$, which is slightly higher than the value predicted in Reference 31. However, the imaginary part of the critical eigenvalue leads to a value of 0·1305 for the frequency, which is relatively close to the one predicted by Ghaddar *et al.*[31] Our direct simulation on mesh 1 led to a fundamental frequency $f_1 = 0{\cdot}130795$. Figure 24 shows the computed eigenvalues and the eigenvector (real and imaginary parts) corresponding to the critical pair of

Table III. Critical eigenvalues

	Re_{cr}	Critical eigenvalue
Mesh 1	1075·5	$0{\cdot}32813 \times 10^{-5} \pm 0{\cdot}82181\mathrm{i}$
Mesh 2	1112·5	$-0{\cdot}23602 \times 10^{-4} \pm 0{\cdot}81995\mathrm{i}$
Mesh 3	1113	$0{\cdot}28909 \times 10^{-4} \pm 0{\cdot}82007\mathrm{i}$

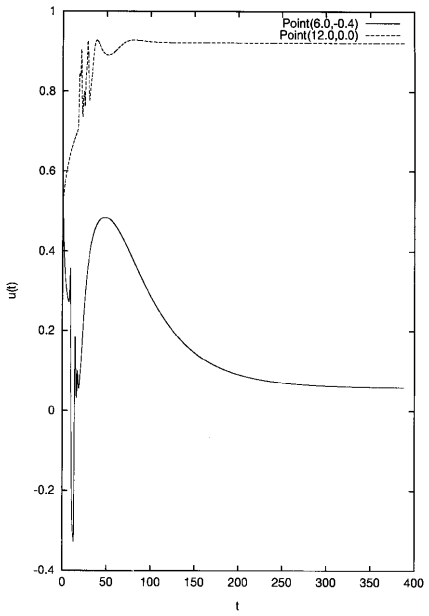

Figure 18. Time evolution of horizontal velocity component at $Re = 800$

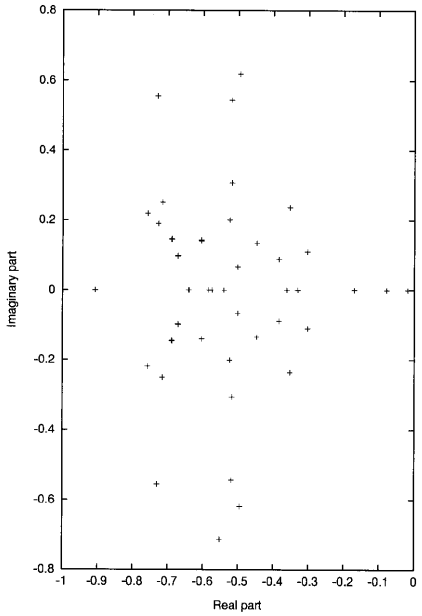

Figure 19. Spectrum of BFS at $Re = 800$ (2000-element mesh)

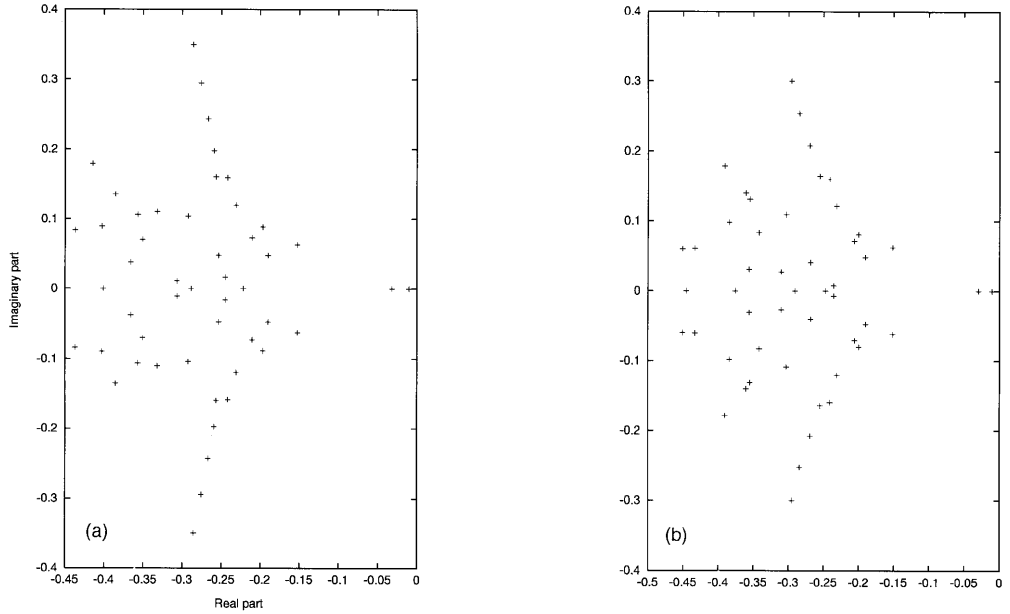

Figure 20. Spectra of BFS at $Re = 1600$: (a) 2000-element mesh; (b) 4200-element mesh

eigenvalues. It is clearly seen that the eigenvector is a perturbation of the classical Tolmien–Schlichting waves of the Poiseuille flow.[31]

Finally, we have conducted a time-dependent simulation at $Re = 1000$ using mesh 1 of Figure 23. The time evolution of the horizontal velocity component is depicted in Figure 25. This last figure shows a significant decrease in the amplitude of the signal. This indicates that the flow is stable for $Re = 1000$ and therefore the flow is also stable for $Re = 975$. At $Re = 1075{\cdot}6$, another simulation shows an oscillating velocity signal, leading to a closed curve in the phase portrait of Figure 26 and to

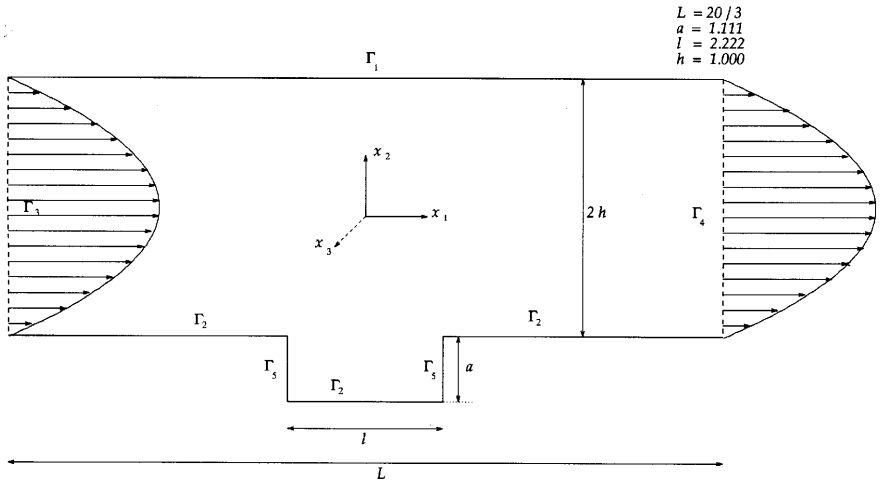

Figure 21. Geometry of grooved channel

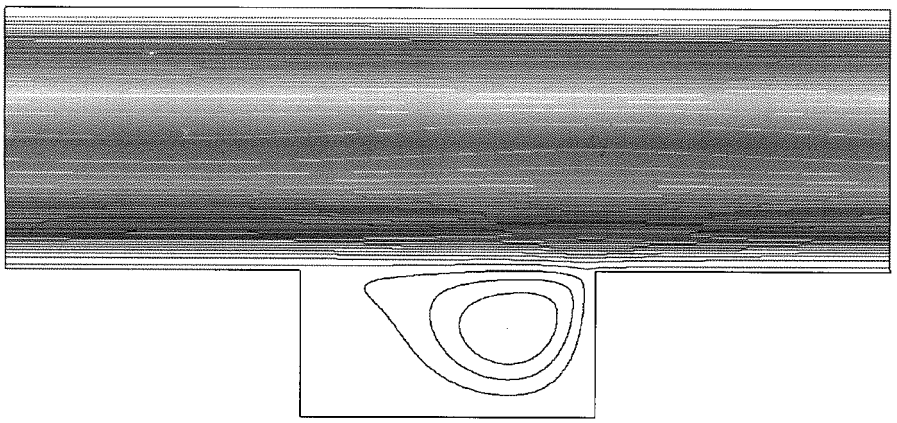

Figure 22. Stationary solution at $Re = 1113$ (mesh 3)

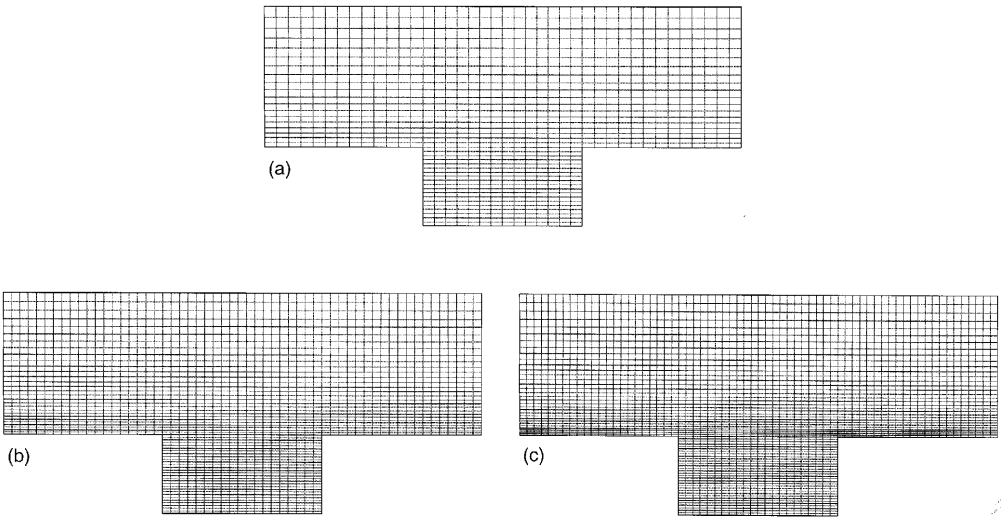

Figure 23. Meshes (a) 1, (b) 2 and (c) 3 for periodic grooved channel

the power spectrum of Figure 27. We can easily conclude that the signal is periodic with a very weak amplitude, indicating that the Hopf bifurcation has just occurred.

6. CONCLUSIONS

We have shown that the method developed in Reference 1 for the computation of eigenvalues and eigenvectors in the Poiseuille flow can be applied to more general problems, especially those where the steady solution is not known analytically. Various two-dimensional flow problems with different boundary conditions were treated. The presence of a Hopf bifurcation has been clearly established in two cases and the results are convergent with mesh refinement.

The proposed method allows the localization of the Hopf bifurcation with greater precision and efficiency than achieved by direct simulation of the time-dependent Navier–Stokes equations.

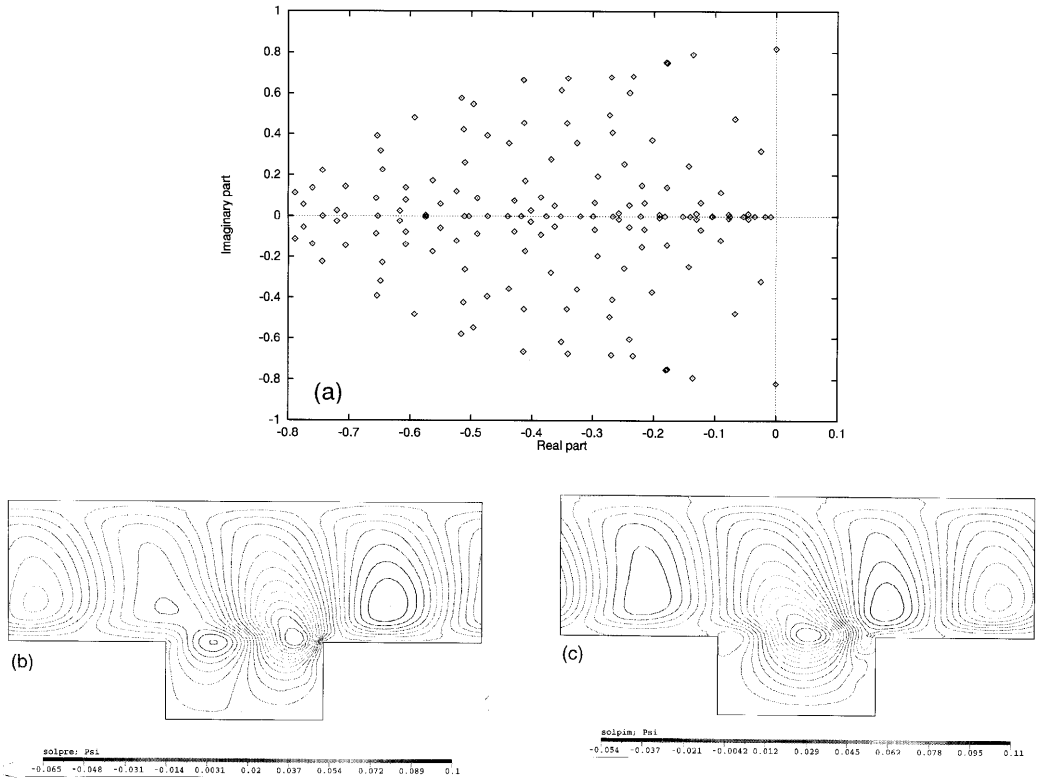

Figure 24. (a) Eigenvalues and (b) real and (c) imaginary parts of critical eigenvector at $Re = 1113$ (mesh 3)

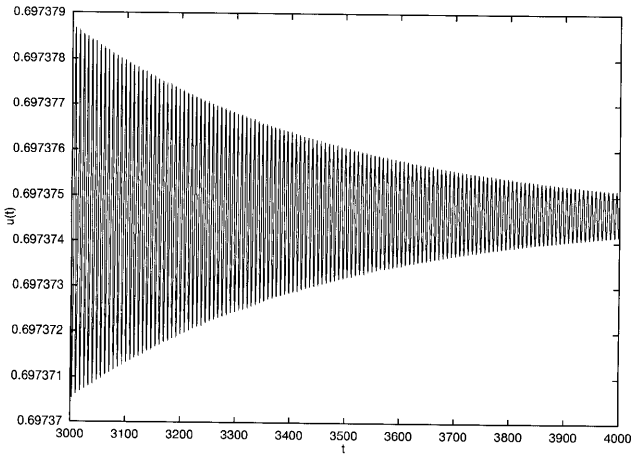

Figure 25. Velocity signal at $Re = 1000$

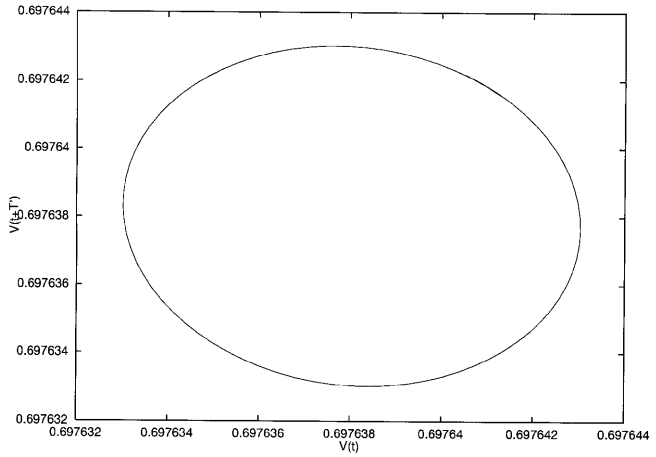

Figure 26. Phase portrait at $Re = 1075{\cdot}5$ (mesh 1)

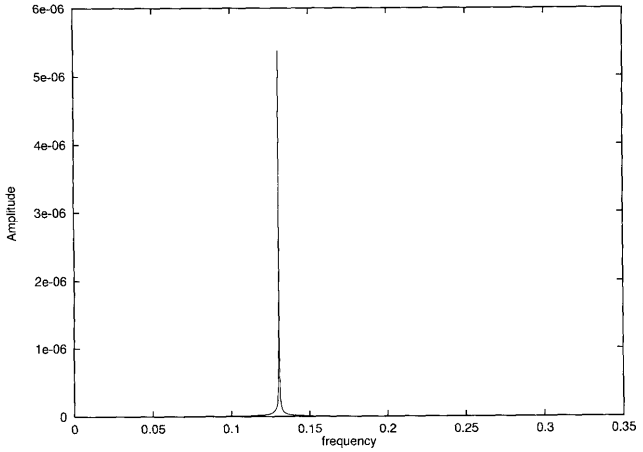

Figure 27. Power spectrum at $Re = 1075{\cdot}6$ (mesh 1)

REFERENCES

1. A. Fortin, M. Jardak, J. J. Gervais and R. Pierre, 'Old and new results on the two-dimensional Poiseuille flow', *J. Comput. Phys.*, **115**, 455–469 (1994).
2. A. Fortin, M. Fortin and J. J. Gervais, 'Complex transition to chaotic flow in a periodic array of cylinders', *Theor. Comput. Fluid Dyn.*, **3**, 79–93 (1991).
3. J. W. Goodrich, K. Gustafson and K. Halasi, 'Hopf bifurcation in the driven cavity', *J. Comput. Phys.*, **90**, 219–261 (1990).
4. K. Gustafson and K. Halasi, 'Vortex dynamics of cavity flows', *J. Comput. Phys.*, **64**, 279–319 (1986).
5. K. Gustafson and K. Halasi, 'Cavity flow dynamics at higher Reynolds number and higher aspect ratio', *J. Comput. Phys.*, **70**, 271–283 (1987)
6. P. M. Gresho, D. K. Gartling, J. R. Torczynsi, K. A. Cliffe, T. J. Garratt, A. Spence and J. W. Goodrich, 'Is the steady viscous incompressible two-dimensional flow over a backward-facing step stable at $Re = 800$?' *Int. j. numer. methods fluids*, **17**, 501–541 (1993).
7. J. J. Gervais, D. Lemelin and R. Pierre, 'Some experiments with stability analysis of discrete incompressible flows in the lid-driven cavity', *Int. j. numer. methods fluids*, **24**, 477–492 (1997).
8. K. Winters, 'Bifurcation and stability, a computational approach', *Comput. Phys. Commun.*, **65**, 299–309 (1991).

9. J. Guckenheimer and P. Holmes, *Nonlinear Oscillations, Dynamical Systems, and Bifurcations of Vector Fields*, Springer, New York, 1983.
10. M. Jardak, *Ph.D. Thesis*, École Polytechnique de Montréal, 1995.
11. F. Brezzi and M. Fortin, *Mixed and Hybrid Finite Element Methods*, Springer, New York, 1991.
12. A. Georgescu, *Hydrodynamic Stability Theory*, Martinus Nijhoff, 1985.
13. A. Jennings, *Matrix Computation for Engineers and Scientists*, Wiley, London, 1977.
14. W. J. Stewart and A. Jennings, 'A simultaneous iteration algorithm for real matrices', *ACM Trans. Softw.*, **7**, 230–242 (1981).
15. K. L. Bathe and E. L. Wilson, *Numerical Methods in Finite Element Analysis*, Prentice-Hall, Englewood Cliffs, NJ, 1976.
16. M. Fortin and A. Fortin, 'Experiments with several elements for viscous incompressible flows', *Int. j. numer. methods fluids*, **5**, 911–928 (1985).
17. M. Fortin, 'Old and new finite elements for incompressible flows', *Int. j. numer. methods fluids*, **1**, 347–364 (1981).
18. K. A. Cliffe, T. J. Garratt and A. Spence, 'Eigenvalues of discretized Navier–Stokes equation with application to the detection of Hopf bifurcations', *Adv. Comput. Math.*, **1**, 337–356 (1993).
19. R. Neubert, 'Predictor–corrector techniques for detecting Hopf bifurcation points', *Bifurc. Chaos Appl. Sci. Eng.*, **3** 1311–1318 (1993).
20. Y. Saad, 'Chebychev acceleration techniques for solving non-symmetric eigenvalue problems', *Math. Comput.*, **42**, (1984).
21. D. C. Sorenson, 'Implicit application of polynomial filters in a *K*-step Arnoldi method', *SIAM J. Matrix Anal. Appl.*, **13**, 357–385 (1992).
22. I. S. Duff and J. A. Scott, 'Computing selected eigenvalues of sparse unsymmetric matrices using subspace iteration', *ACM Trans. Math. Softw.*, **19**, 137–159 (1991).
23. K. A. Cliffe, T. J. Garratt and A. Spence, 'Eigenvalues of block matrices arising from problems in fluid mechanics', *SIAM J. Matrix Anal. Appl.*, **15**, 1310–1318 (1994).
24. A. Griewank and G. Reddien, 'The calculation of Hopf points by a direct method', *IMA J. Numer. Anal.*, **3**, 295–304 (1983).
25. M. Fortin and A. Fortin, 'A generalizatin of Uzawa algorithm for the solution of the Navier–Stokes equations', *Commun. Appl. Numer. Methods*, **1**, 205–208 (1985).
26. S. A. Orszag, 'Accurate solution of the Orr–Sommerfeld stability equation', *J. Fluid Mech.*, **50**, 689–703 (1971).
27. K. Gustafson, 'Theory and computation of periodic solutions of autonomous partial differential equation boundary value problems, with application to the driven cavity', *Math. Comput. Model*, **22**, 57–75 (1995).
28. C. H. Bruneau and C. Jouron, 'Un nouveau schéma décentré pour le problème de cavité entraînée', *C. R. Acad. Sci. Paris*, **307**, 359–362 (1988).
29. J. Shen, 'Hopf bifurcation of the unsteady regularized driven cavity flow', *J. Comput. Phys.*, **95**, 228–245 (1991).
30. L. Kaiktsis, G. E. Karniadakis and S. Orszag, 'Onset of three-dimensionality, equilibria and early transition in the flow over a backward facing step', *J. Fluid Mech.*, **231**, 501–528 (1991).
31. N. K. Ghaddar, K. Z. Korczak, B. B. Mikic and A. T. Patera, 'Numerical investigation of incompressible flow in grooved channel, Part 1. Stability and self-sustained oscillations', *J. Fluid Mech.*, **163**, 99–127 (1986).
32. A. Fortin, On the imposition of a flowrate by an augmented Lagrangian method', *Commun. Appl. Numer. Methods*, **4**, 835–841 (1988).
33. D. K. Gartling, 'A test problem for outflow boundary conditions', *Int. j. numer. methods fluids*, **11**, 953–967 (1990).

